



# Design and Optimization of a Broadband Waveguide-to-50 $\Omega$ -Microstrip Transition for Q-Band Applications with Low-Loss and Easy Scalability

Diana Cubillos<sup>1,2</sup> · Camilo Espinoza<sup>3</sup> · David Monasterio<sup>3</sup> · José Pizarro<sup>3</sup> · Leonardo Bronfman<sup>3</sup> · Ricardo Finger<sup>3</sup> · F. Patricio Mena<sup>1,4</sup>

Received: 11 April 2023 / Accepted: 10 July 2023

© The Author(s), under exclusive licence to Springer Science+Business Media, LLC, part of Springer Nature 2023

## Abstract

The increment in the demand for high-frequency monolithic integrated circuits has driven the development of waveguide-to-microstrip transition that allow their characterization and integration with waveguide components. Unfortunately, when return losses are taken into account, these transitions feature a rather narrow bandwidth, especially when the substrate is inserted transversal to the propagation direction of the waveguide. Here, we present a new scalable design that overcomes this problem. The transition was originally designed for a bandwidth of 33.5–60 GHz (extended V-band) with the simulation results showing reflections below  $-19.5$  dB in a fractional bandwidth of 55%. To validate the design, we show the scaling, construction, and measurement in an extended Q-band (27–50 GHz) with the additional advantage of having a standard impedance of 50  $\Omega$ . The most novel feature is a staggered air cavity for the microstrip and planar probe, which generates return losses better than 20 dB in a fractional bandwidth of 53%.

**Keywords** Impedance Transformer · Q-band · Rectangular Waveguide · Waveguide-to-microstrip Transition

## 1 Introduction

Integrated circuits at the microwave ranges are increasingly used in areas such as communications [1, 2], radar [3, 4], and on radio astronomy [5–7]. Most of these circuits are fabricated on planar microstrip substrates, which require transitions to waveguide for two main reasons. First, to connect the circuits with waveguides that allow their characterization in waveguide-based setups. Second, for their integration with waveguide components such as high-gain antennas [8], diplexers [9], filters [10], and orthomode transducers [11]. In our particular case, the transition is needed

---

Extended author information available on the last page of the article

for the transmission of the LO signal within a sub-harmonic mixer that is currently being developed for an extended W-band (67–116 GHz). Thus, the development of transitions between planar transmission lines and rectangular waveguides is of vital importance.

Several types of transitions have been proposed to satisfy this need. They vary on geometry and functional bandwidth but can roughly be classified into two groups according to the relative position between the waveguide and the microstrip. The first group can be referred to as inline transitions, where the substrate is inserted in the propagation direction of the waveguide [12–16] and can be placed either parallel to the E- or the H-plane. These types of transitions are compact but have a narrow bandwidth. A slightly wider bandwidth can be obtained if a stepped ridged waveguide or gradual tapering of an antipodal fin-line is used [17].

In the second group, the substrate is inserted through the broadwall of the waveguide, parallel (E-plane) or transversal to the propagation direction of the waveguide [18–23]. These types of transitions are larger due to the layout of the ports, but, in the case of E-plane transitions, they can achieve large fractional bandwidths (45%) [20]. Transversal transitions, on the other hand, have narrower bandwidths (31%) [24] with some exceptions like those having reduced height waveguide (44%) [25] or suspended stripline (SSL) (41%) [26]. However, due to their port layout, the latter are more difficult to integrate into planar circuits.

State-of-the-art applications, especially in radio astronomy, are requiring even larger operational bandwidths, some exceeding 50% with the added requirement of achieving return losses of around  $-20$  dB [27, 28]. Achieving this feat for every component of a given microwave system is, however, extremely difficult and even more so at the mm and sub-mm ranges, [29–31]. Here, we present a new scalable microstrip-to-waveguide transition that meets these stringent requirements. It has a return loss better than  $-19.5$  dB in a fractional bandwidth of 55% and is easy to integrate with planar circuits. The original design was made in the V-band, but to demonstrate its capabilities, a prototype was developed in the range of 27–50 GHz, which is 35% larger than the full Q-band. The transition consists of a stepped transformer and a dendritic probe printed over a dielectric substrate, which is inserted into a rectangular waveguide containing a backshort. Importantly, the output port is a microstrip with a standard impedance of  $50 \Omega$  which facilitates its integration with printed circuits. Using a back-to-back transition, we demonstrate low insertion and good return losses across the entire band.

## 2 Design and Simulations

The transition was simulated and optimized using an electromagnetic analysis tool (Ansys HFSS). The model uses a 0.127 mm thick RT/Duriod 6002 dielectric substrate with nominal relative permittivity and tangent loss values of 2.94 and 0.0012, respectively.

## 2.1 Justification of the Design

The final layout of the transition, obtained after the design process discussed in Sec. 2.3, is presented in Fig. 1. The incoming signal enters the waveguide port (1) and is followed by a  $\lambda/4$ -waveguide transformer (2) in order to adapt it to a non-standard waveguide (3). The latter is used to increase the coupling between the waveguide and the probe antenna. A non-standard waveguide is used since, as demonstrated in [32], the fundamental-mode impedance can be adjusted by selecting properly its dimensions  $a$  and  $b$  according to

$$Z_{0_{TE_{10}}} = \frac{4b}{a} \frac{\eta}{\sqrt{1 - \left(\frac{c}{2af}\right)^2}}, \quad (1)$$

where  $\eta$  is the characteristic impedance of free space,  $c$  is the speed of light, and  $f$  is the frequency. In particular, this waveguide allows to extend the operational bandwidth at the lower end, close to the cut-off frequency of the input waveguide port. After the non-standard waveguide, an adaptation (4) is introduced in order to reduce the disturbance of the fundamental mode when it couples with the probe antenna (5). Then, the waveguide is terminated in a short circuit in the form of a backshort (6) that allows to couple the reflected power to the probe with the correct phase.

The electromagnetic field in the probe antenna is conducted, first, through a transmission line with a small air cavity that behaves effectively as a double-layer stripline (7), where a quasi-TEM mode is propagated. This type of line is appropriate because its compactness minimizes the disturbance in the electric fields of the fundamental mode and in the surface currents in the wide wall of the waveguide.

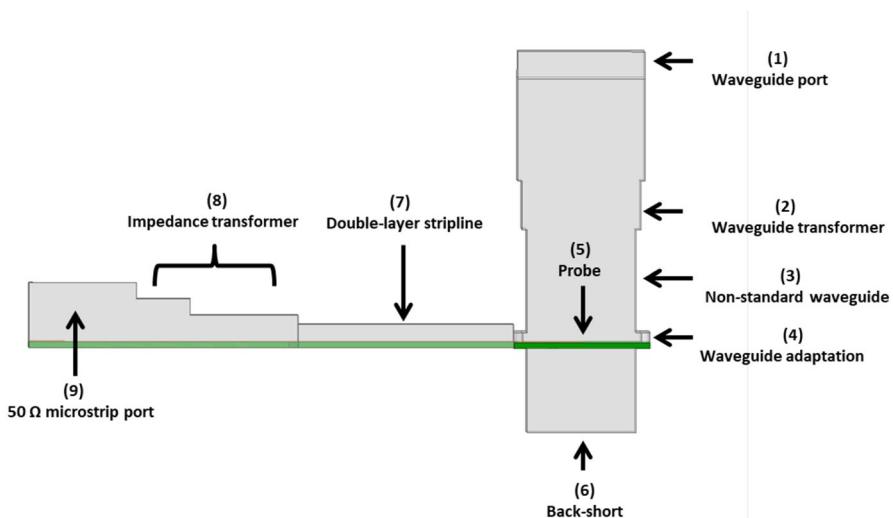


**Fig. 1** General layout of the transition with its different parts. The function of each part is discussed in the text (Sec. 2.1)

Finally, a two-step impedance transformer (8) with an expanding cavity is used to obtain a proper microstrip line with a standard 50- $\Omega$  impedance (9). Through simulations (see Sec. 2.3), it was demonstrated that this morphology is capable of increasing the operational bandwidth of the transition, especially at the lower end.

## 2.2 Optimization of the Probe Antenna

Several candidates, such as [20, 24, 26, 33, 34], can be used as antenna probe. Through simulations, the performance of a radial probe was contrasted against a dendritic probe within a simplified version of the structure presented here. The results showed a slight better performance for the dendritic probe. Therefore, we selected that design as the base from which we developed the proposed structure. During the entire design process, that will be explained in the following section, optimization of its dimensions provided no significant changes to the electrical behavior of the transition. Under those circumstances, the probe remained the same over the entire design process.

## 2.3 Original V-Band Design

The transition was designed to carry local oscillator (LO) signal (33.5–58 GHz) to a sub-harmonic mixer. The design process went through four stages, as shown in Fig. 2, that allowed to achieve the greatest possible bandwidth coverage. On the one hand, the dimensions of the metal structure of the entire transition change with each stage. The thickness of the substrate and the conductor were kept constant. Improving simulated reflections in each step can be seen in Fig. 3.

Figure 2a shows the initial geometry of the transition with standard WR-19 waveguide dimensions and a dielectric substrate. The size of the air cavity above the microstrip was optimized achieving reflection losses in a fractional bandwidth of 42%. In the next stage, Fig. 2b, a larger waveguide section located above the substrate in the cross-section of the waveguide was included. The fractional bandwidth was increased to 46%. In the third stage, Fig. 2c, the dimensions of the waveguide and the backshort were modified. Dimensions W1 and L2 dimensions were found to allow increasing the fractional bandwidth to 55%. However, this change generated an increase in reflections between 45 and 55 GHz that is caused by the impedance mismatch between the waveguide and the port. Finally, in Fig. 2d, a waveguide transformer (L1) was used to match dimension (L2) with port WR-19. This transformer made it possible to achieve a bandwidth of 55% with reflections below –20 dB in almost the entire required frequency range. In addition, a two-step impedance transformer was used to achieve the standard 50- $\Omega$  impedance at the microstrip port.

Figure 4a shows the final design of the transition which consists of four parts. The first is a waveguide transformer with three sections (H1 to H3) that allows connection to a standard waveguide and a backshort to prevent radiation from the guide terminal. Secondly, the union of two sections of the waveguide (H4 and H6) where the change from the TE<sub>10</sub> modes to quasi-TEM is generated. Third, a two-step impedance matcher (H7 and H8) provides the standard impedance at the output port.

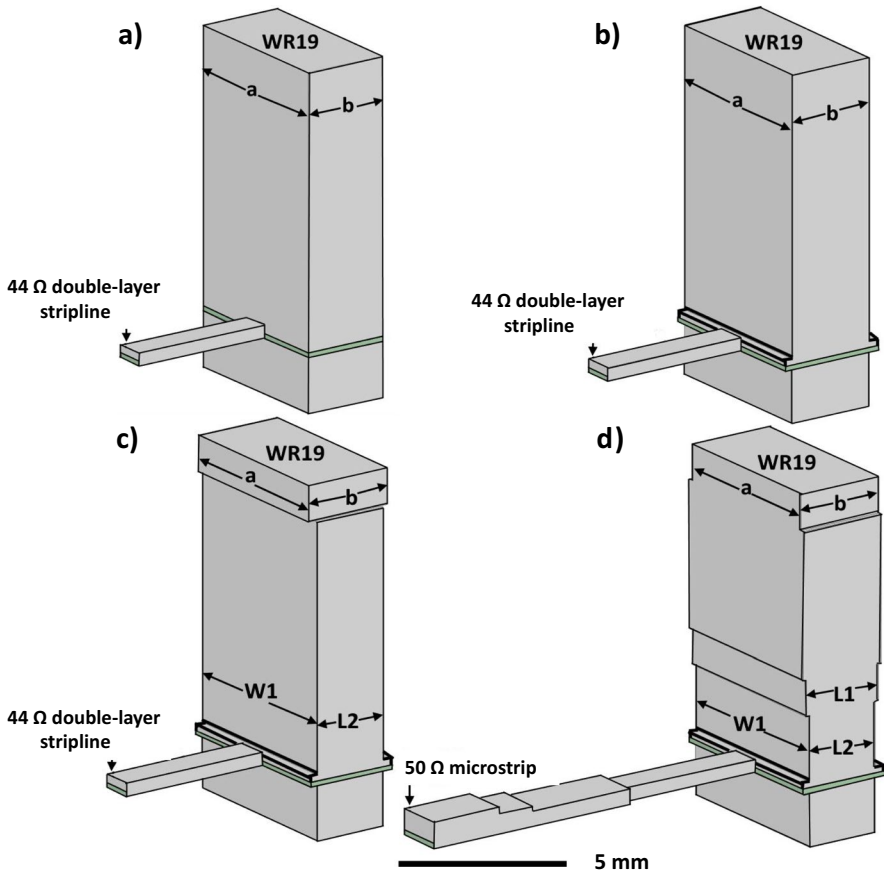


**Fig. 2** Design process of the transition for V-band. While the dimensions of the metal structure of the entire transition change with each stage, those of the probe are kept constant. **a** Waveguide and backshort in WR-19 dimensions with microstrip output. **b** A wider waveguide section on the substrate is added in the cross-section of the waveguide to increase the bandwidth without modifying the size of the waveguide. **c** Waveguide dimensions ( $W1$  and  $L2$ ) are optimized to reduce reflections. **d** A waveguide transformer ( $L1$ ) is added to decrease reflections due to a mismatch between port WR-19 and waveguide ( $L2$ ). A two-step impedance adapter is used to achieve standard impedance on the microstrip output port

Finally, the fourth part is a dielectric substrate with a second-order dendritic probe (Fig. 4b).

## 2.4 Scaling to Q-Band

To validate the design discussed in the previous section, the transition was scaled to the Q-band. The physical dimensions obtained after software optimization are given in Table 1. This process demonstrates that except for the microstrip, the design of this transition can be adapted to different frequencies by scaling the entire structure by a factor that depends on the required

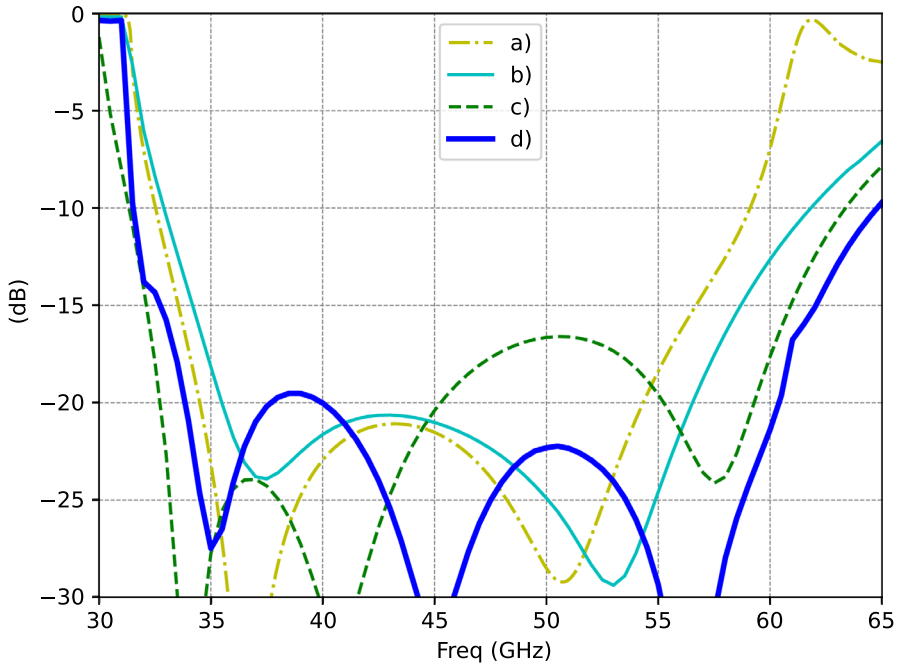


**Fig. 3** Reflection losses of each stage a) to d) in the evolution of the V-band transition design presented in Fig. 2. The improvement in the bandwidth of the reflections with each stage is evident. The final design stage shows a return loss near to  $-20$  dB in the entire bandwidth

frequency. In this case, the scale factor was the result of the quotient between the minimum frequency for the WR-19 and WR-22 waveguides. In contrast, the microstrip line requires a redesign based on the characteristics of the substrate.

The simulation results are shown in Fig. 5. The maximum insertion loss is 0.31 dB, and the corresponding return loss is better than  $-20$  dB in the frequency range of 27 to 50 GHz. In addition, a modal analysis was performed and no high-order modes were found to be excited at relevant levels. The optimization process showed that the most critical dimensions are the distance to the waveguide (L4) and the height difference (H6–H4). They have tolerances of  $\pm 50$  and  $\pm 100$   $\mu\text{m}$ .

### 3 Implementation and Characterization of the Q-Band Transition

To accurately determine the transition losses, it is necessary to discount the microstrip line losses from the measured transition losses. Therefore, characterization of the substrate and the transition are required.

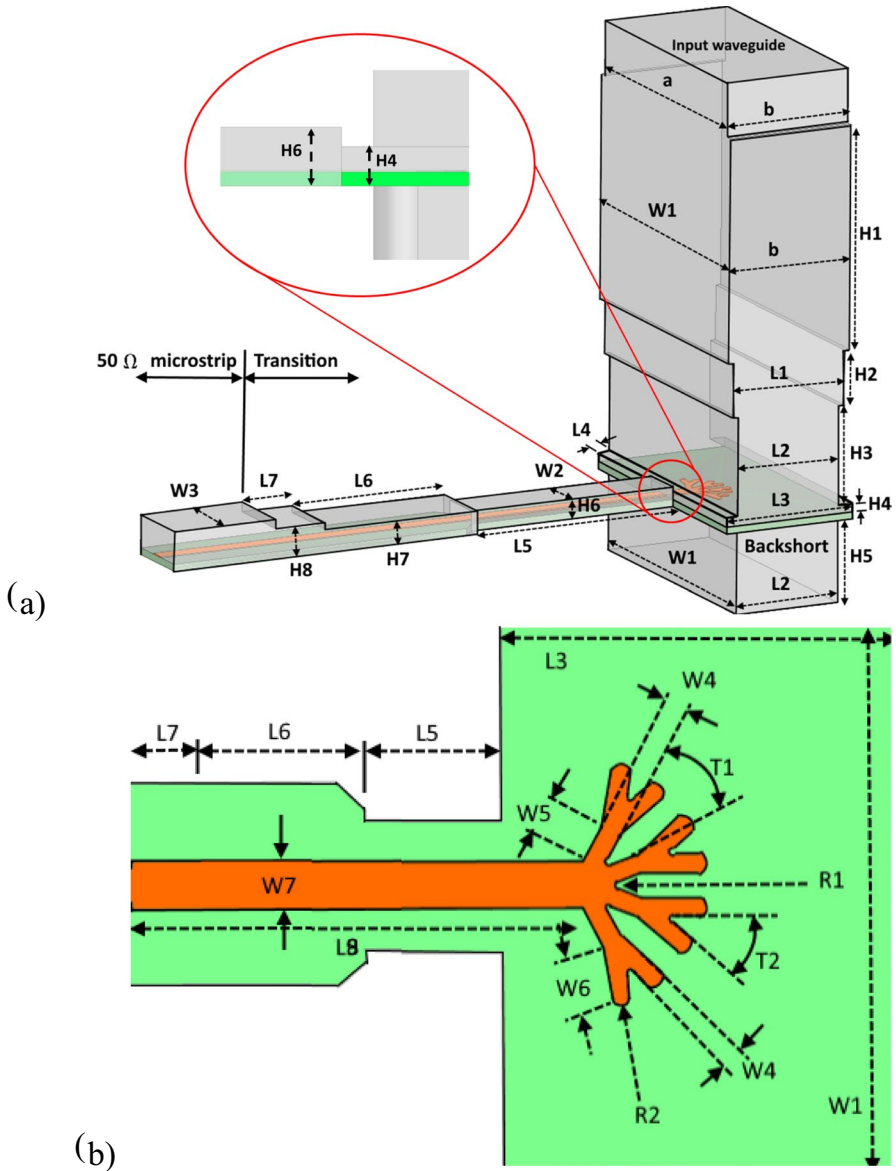


**Fig. 4** **a** Three-dimensional view of the transition structure. The inset shows the union of the two waveguide sections H4 and H6. **b** Substrate, conductive line, and dendritic probe

### 3.1 Back-to-Back Experiment for Substrate Characterization

To determine the loss tangent of the substrate, two lines of different lengths (40 and 50 mm) were mounted back-to-back as shown in Fig. 6a. The lines were

**Table 1** Dimensions of transition

H1	2.3	H7	0.73	L5	4.84	W3	1.59	R1	0.02
H2	1.09	H8	1.10	L6	2.42	W4	0.14	R2	0.05
H3	2.3	L1	2.66	L7	1.21	W5	0.3	T1	41°
H4	0.23	L2	2.44	L8	9.09	W6	0.42	T2	40°
H5	1.89	L3	3.06	W1	5.9	W7	0.34		
H6	0.53	L4	0.29	W2	1.02	W8	0.31		

All dimensions in mm unless indicated otherwise

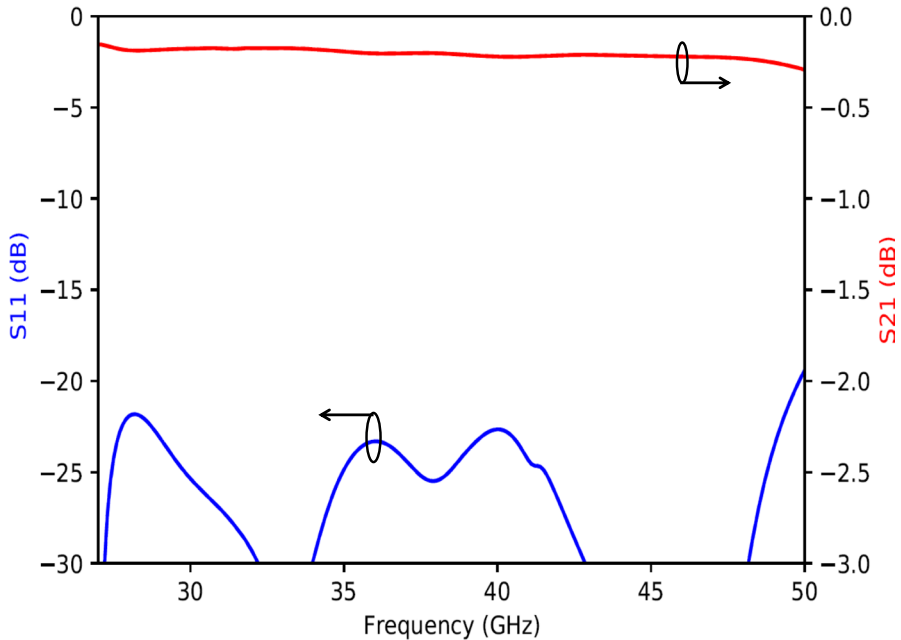


**Fig. 5** Simulated scattering parameters of the Q-band transition. The dielectric substrate used in the simulations was RT/Duroid 6002 with nominal values of relative permittivity (2.94) and loss tangent (0.0012) given by the manufacturer. The maximum insertion loss is 0.31 dB and the return loss is better than  $-20$  dB in the frequency range from 27 to 50 GHz

manufactured using an LPKF ProtoLaser S laser machine, and their return and insertion losses were measured using an Agilent PNA Network Analyzer E8364C.

### 3.2 Back-to-Back Experiment for Measurements of Transition

To experimentally validate the simulation results, a back-to-back transition for Q-band was fabricated, as shown in Fig. 6b and c. The transition was characterized with the same instrument but calibrated utilizing an Agilent TRL calibration kit 11644A.

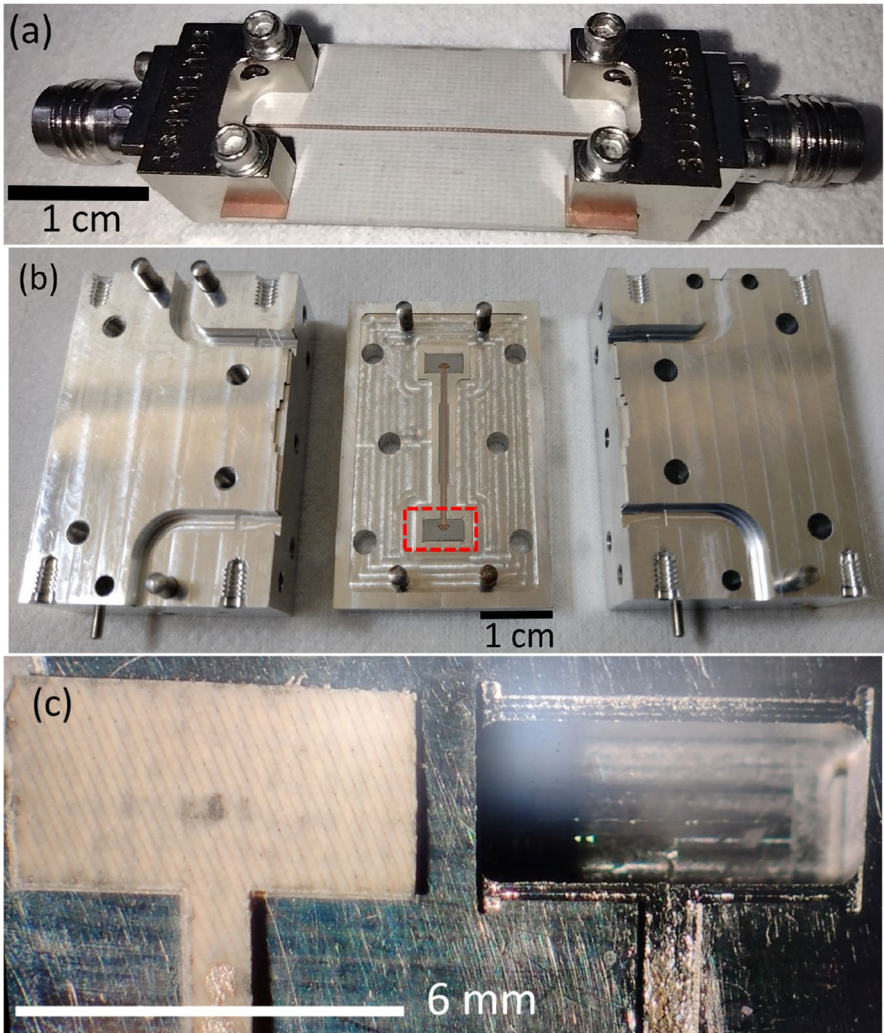


**Fig. 6** **a** Simple microstrip line for substrate characterization. **b** Back-to-back block containing the Q-band transition. The block was fabricated out of three aluminum parts, two of them forming the waveguide structure and the third containing the dielectric substrate and backshort. The red-dashed box indicates the area shown in the next panel. **c** Bottom block with the substrate removed to indicate how the latter is placed. In the final assembly, the substrate is suspended above the cavity. The substrate is adhered to the block with silver conductive epoxy with no further alignment

## 4 Results and Discussion

### 4.1 Substrate Characterization

Utilizing the measurements of the two microstrip lines (40 and 50 mm) and the difference in their S parameters, the losses of the connectors were discounted. Then,

considering a constant relative electrical permittivity of 2.94, we calculated a loss tangent of  $0.01626 \pm 0.0020$ , which is considerably higher than reported in the substrate datasheet. Although the fabrication process seems to have altered the properties of the substrate, further studies, beyond the scope of this work, are necessary to find the precise cause of this difference.

## 4.2 Back-to-Back Transition

The solid lines in Fig. 7 show the measured results of the scattering parameters of the back-to-back transition for the final design. The maximum insertion loss is 3.2 dB and the corresponding return loss is better than 20 dB between 28.5 and 49.1 GHz with a fractional bandwidth of 53%.

The back-to-back simulation was performed again using the measured loss tangent from the microstrip experiment. These results are presented in the dashed lines of Fig. 7. A good agreement with the measurements can be seen, which means that the measured excess insertion losses are the result in the increase of the effective loss of the structure. Regarding the return loss, the disagreement between simulation and measurements at both edges of the band is attributed to tolerances in machining and in the assembly process of the dielectric substrate into the block.

To discount the effect of the microstrip line on the results, we followed the method described in references [15, 17, 18, 21, 24, 34–36], which includes

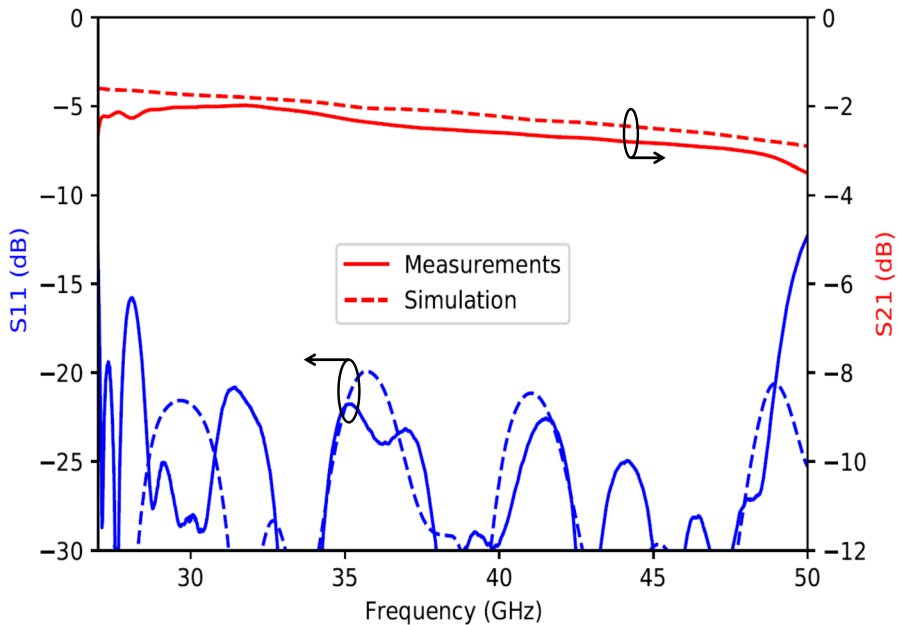


**Fig. 7** Measured and simulated scattering parameters of the back-to-back Q-band transition. In contrast with the simulations presented in Fig. 2, these simulations were made using the measured values of permittivity (2.94) and loss tangent (0.01626) calculated from the microstrip line measurements

estimating the losses of the transmission line that connect to the antennas. Through simulations in HFSS using the measured loss tangent in the microstrip experiment, the value of maximum insertion loss for the 22 mm microstrip line was estimated in  $\sim 2.6$  dB. Using the maximum measured losses of the back-to-back ( $L_b$ ), the maximum simulated losses of the 22 mm microstrip line ( $L_m$ ) and considering the symmetry, the maximum losses for a single transition are  $(L_b - L_m)/2 = (3.2\text{dB} - 2.6\text{dB})/2 = 0.3\text{dB}$  which agrees with the value from the simulations. Finally, in Table 2, we compare the performance of the transition presented in this work with other transitions at different frequency ranges. In addition, Fig. 8 shows the comparison with other transitions regarding return losses, attenuation, and fractional bandwidth. The advantages of the proposed transition are evident.

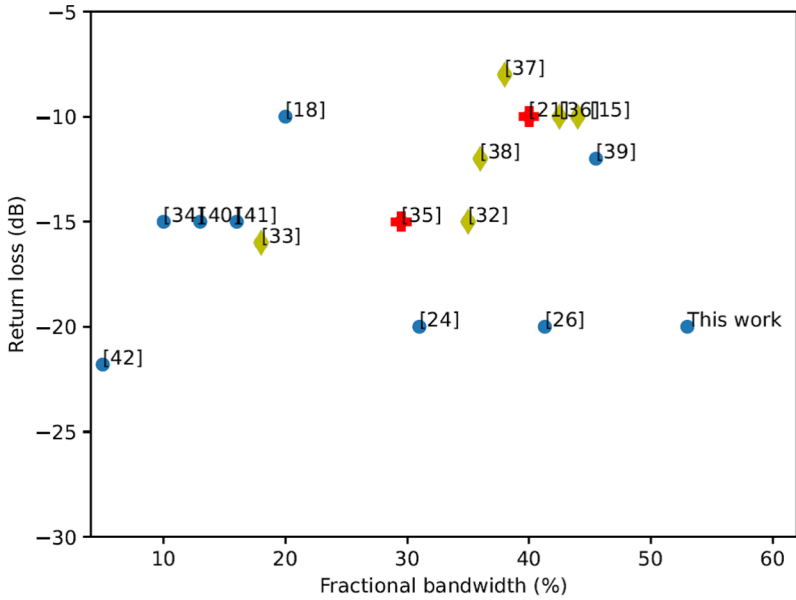
## 5 Conclusions

In this work, we have presented the design, simulation, and measurements of a scalable ultra-bandwidth transition from waveguide to  $50\text{-}\Omega$  microstrip line. The design was implemented using a standard WR-22 waveguide, achieving a fractional bandwidth of 53%, significantly larger than the standard waveguide coverage of 40% (33–50 GHz). Importantly, this extended bandwidth was achieved without exciting any other high-order mode by obtaining an excellent reflection in the bandwidth where only the fundamental mode is propagated. The transition presents a novel

**Table 2** Comparisons between this work and other reported transitions (*RL* return losses, *IL* insertion losses, *TL* total loss, *AT* attenuation)

Ref	Freq (GHz)	Type	FBW(%)	RL (dB)	IL (dB)	AT (dB)
[37]	26–40	Inline-H	42.5	$\leq -10$	$< 0.33$	$-20.32$
[33]	75–110	Inline-E	38	$\leq -8$	$< 0.63$	$-14.84$
[15]	31–48	Inline-E	44	$\leq -10$	$< 1.7$	$-6.29$
[38]	50–72	Inline-E	36	$\leq -12$	$< 0.35$	$-19.31$
[35]	27–39	Inline-E	35	$\leq -15$	$< 0.5$	$-15.86$
[17]	40–48	Inline-E	18	$\leq -16$	$< 0.5$	$-15.84$
[21]	33–50	E-plane	40	$\leq -10$	$< 0.36$	$-19.46$
[36]	37–50	E-plane	29.5	$\leq -15$	$< 0.25$	$-22.27$
[18]	40–50	Transversal	20	$\leq -10$	$< 0.15$	$-28.69$
[39]	49–77	Transversal	45.5	$\leq -12$	$< 0.5$	$-16.01$
[34]	40–50	Transversal	10	$\leq -15$	$< 0.3$	$-20.55$
[40]	26–28	Transversal	13	$\leq -15$	$< 0.2$	$-24.41$
[41]	26–31	Transversal	16	$\leq -15$	$< 0.8$	$-11.80$
[24]	27–37	Transversal	31	$\leq -20$	$< 0.2$	$-24.31$
[26]	26–40	Transversal	41.3	$\leq -20$	$< 0.15$	$-27.08$
[42]	38–40	Transversal	5	$\leq -21.8$	$< 0.58$	$-14.50$
This work	28–49	Transversal	53	$\leq -20$	$< 0.3$	$-20.48$

a)



b)

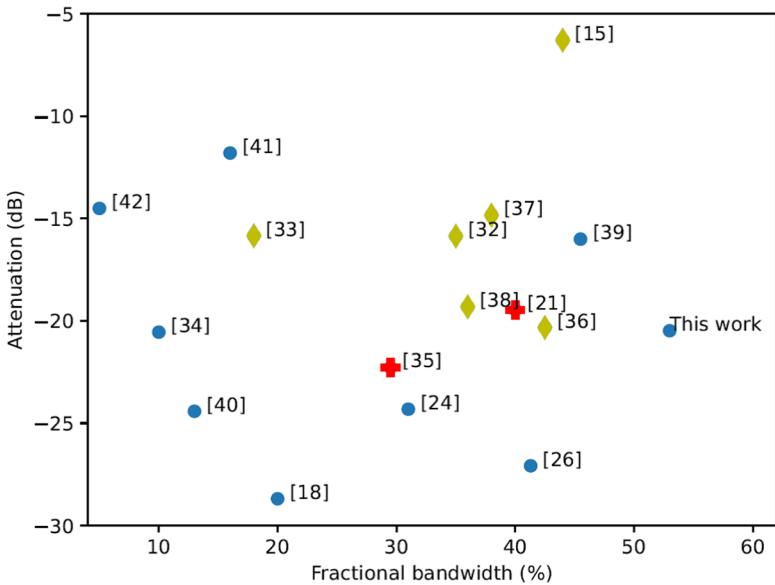


**Fig. 8** Graphic representation of Table 2. Each marker represents a different type of transition. Diamonds are for inline, crosses for E-plane, and dots for transversal. **a** Reflection loss versus fractional bandwidth. **b** Attenuation versus fractional bandwidth. The excellent performance of the transition presented here is evident

structure that allows this extreme bandwidth increase, specially at the lower edge of the bandwidth, where reflections produced by the natural waveguide cut-off region are significant. The proposed design was compared to other works, presenting the largest fractional bandwidth with the lowest return loss, making it ideal for applications where matching between components is important, such as radio astronomy. Moreover, the 50- $\Omega$  microstrip allows seamless integration with other components such as microwave-integrated circuits, making it ideal for applications where ultra-bandwidth mixers and low-noise amplifiers are used.

**Author Contribution** C. Espinoza, D. Monasterio, and D. Cubillos designed the block. J. Pizarro machined the block. C. Espinoza and D. Cubillos joined the block. D. Monasterio and D. Cubillos made the measurements. F.P. Mena, D. Monasterio, R. Finger, and D. Cubillos did the data analysis. D. Cubillos wrote the draft. Finally, all the authors reviewed and edited the draft.

**Funding** We acknowledge the support of Chilean Agencia Nacional de Investigación y Desarrollo (ANID) under grants Basal Projects ACE210002 and FB210003, ALMA-ANID 31180005, FONDECYT 1180700, 1221662 and FONDEF ID21-10359. The work of D. Monasterio was supported by CONICYT-PFCHA/Doctorado Nacional/2019–2119063.

**Data Availability** The data that support the findings of this study are available from the corresponding author, D. C., upon reasonable request.

## Declarations

**Ethical Approval** Not applicable.

**Competing Interests** The authors declare no competing interests.

## References

1. Rappaport, T.S., Sun, S., Mayzus, R., Zhao, H., Azar, Y., Wang, K., Wong, G.N., Schulz, J.K., Samimi, M., Gutierrez, F.: Millimeter Wave Mobile Communications for 5G Cellular: It Will Work! *IEEE Access* **1**, 335–349 (2013) <https://doi.org/10.1109/ACCESS.2013.2260813>
2. Mao, C.-X., Khalily, M., Xiao, P., Brown, T.W.C., Gao, S.: Planar Sub-Millimeter-Wave Array Antenna With Enhanced Gain and Reduced Sidelobes for 5G Broadcast Applications. *IEEE Transactions on Antennas and Propagation* **67**(1), 160–168 (2019) <https://doi.org/10.1109/TAP.2018.2874796>
3. Cheng, B., Lu, B., Gao, J., Chen, P., Liu, Q., He, Y., He, X.: Standoff 3-D imaging with 4Tx-16Rx MIMO-Based radar at 340 GHz. In: 2017 42nd International Conference on Infrared, Millimeter, and Terahertz Waves (IRMMW-THz), pp. 1–2 (2017). <https://doi.org/10.1109/IRMMW-THz.2017.8067176>
4. Paik, S.F.: MMIC radar transceivers for industrial sensors. In: Proceedings of 1995 IEEE MTT-S International Microwave Symposium, pp. 1063–10653 (1995). 13
5. Kerr, A.R., Pan, S.-K., Claude, S.M.X., Dindo, P., Lichtenberger, A.W., Effland, J.E., Lauria, E.F.: Development of the ALMA Band-3 and Band-6 Sideband- Separating SIS Mixers. *IEEE Transactions on Terahertz Science and Technology* **4**(2), 201–212 (2014) <https://doi.org/10.1109/THz.2014.2302537>
6. Wu, Y.-C., Hwang, Y.-J., Chiong, C.-C., Lu, B.-Z., Wang, H.: An Innovative Joint-Injection Mixer With Broadband If and RF for Advanced Heterodyne Receivers of Millimeter-Wave Astronomy. *IEEE Transactions on Microwave Theory and Techniques* **68**(12), 5408–5422 (2020) <https://doi.org/10.1109/TMTT.2020.3028965>

7. Graauw, T.: The Atacama Large Millimeter/submillimeter Array. In: 2011 International Conference on Infrared, Millimeter, and Terahertz Waves, pp. 1–4 (2011). <https://doi.org/10.1109/IRMMWvTHz.2011.6105024>
8. Smith, S.L., Merkle, T., Smart, K.W., Hay, S., Shen, M., Ceccato, F.: Design Aspects of an Antenna-MMIC Interface Using a Stacked Patch at 71–86 GHz. *IEEE Transactions on Antennas and Propagation* **61**(4), 1591–1598 (2013) <https://doi.org/10.1109/TAP.2013.2239251>
9. Monasterio, D., Jarufe, C., Gallardo, D., Reyes, N., Mena, F.P., Bronfman, L.: A Compact Sideband Separating Downconverter With Excellent Return Loss and Good Conversion Gain for the W Band. *IEEE Transactions on Terahertz Science and Technology* **9**(6), 572–580 (2019) <https://doi.org/10.1109/TTHZ.2019.2937955>
10. Shen, G., Che, W., Feng, W., Shi, Y., Shen, Y.: Low Insertion-Loss MMIC Bandpass Filter Using Lumped-Distributed Parameters for 5G Millimeter-Wave Application. *IEEE Transactions on Components, Packaging and Manufacturing Technology* **11**(1), 98–108 (2021) <https://doi.org/10.1109/TCPMT.2020.3039987>
11. Valente, G., Navarrini, A., Schaefer, F., Serres, P., Thome, F.: Architecture of Highly Integrated Cryogenic Active Planar OrthoMode Transducer for the 3-mm Band. In: 2018 2nd URSI Atlantic Radio Science Meeting (AT-RASC), pp. 1–4 (2018). <https://doi.org/10.23919/URSI-AT-RASC.2018.8471471>
12. Van Heuven, J.H.C.: A New Integrated Waveguide-Microstrip Transition. In: 1974 4th European Microwave Conference, pp. 541–545 (1974). <https://doi.org/10.1109/EUMA.1974.332108>
13. Yao, H.-W., Abdelmonem, A., Liang, J.-F., Zaki, K.A.: A full wave analysis of microstrip-to-waveguide transitions. In: 1994 IEEE MTT-S International Microwave Symposium Digest (Cat. No.94CH3389-4), pp. 213–2161 (1994). <https://doi.org/10.1109/MWSYM.1994.335341>
14. Wu, C., Zhang, Y., Li, Y., Zhu, H., Xiao, F., Yan, B., Xu, R.: Millimeter-Wave Waveguide-to-Microstrip Inline Transition Using a Wedge-Waveguide Iris. *IEEE Transactions on Microwave Theory and Techniques*, 1–1 (2021) <https://doi.org/10.1109/TMTT.2021.3123349>
15. Lou, Y., Chan, C.H., Xue, Q.: An in-line waveguide-to-microstrip transition using radial-shaped probe. In: 2007 IEEE Antennas and Propagation Society International Symposium, pp. 3117–3120 (2007). <https://doi.org/10.1109/APS.2007.4396196>
16. Zhang, Y., Ruiz-Cruz, J.A., Zaki, K.A., Piloto, A.J.: A Waveguide to Microstrip Inline Transition With Very Simple Modular Assembly. *IEEE Microwave and Wireless Components Letters* **20**(9), 480–482 (2010) [10.1109/LMWC.2010.2056358](https://doi.org/10.1109/LMWC.2010.2056358)
17. Sharma, A.K.: Tunable waveguide-to-microstrip transition for millimeter-wave applications. In: 1987 IEEE MTT-S International Microwave Symposium Digest, vol. 1, pp. 353–356 (1987). <https://doi.org/10.1109/MWSYM.1987.1132403>
18. Shih, Y.-C., Ton, T.-N., Bui, L.Q.: Waveguide-to-microstrip transitions for millimeter-wave applications. In: 1988, IEEE MTT-S International Microwave Symposium Digest, pp. 473–4751 (1988). <https://doi.org/10.1109/MWSYM.1988.22077>
19. Li, E.S., Tong, G.-X., Niu, D.C.: Full W-band Waveguide-to-microstrip Transition With New E-plane Probe. *IEEE Microwave and Wireless Components Letters* **23**(1), 4–6 (2013) <https://doi.org/10.1109/LMWC.2012.2235176>
20. Kooi, J., Chattopadhyay, G., Withington, S., Rice, F., Zmuidzinas, J., Walker, C., Yassin, G.: Full-Height Waveguide to Thin-Film Microstrip Transition with Exceptional RF Bandwidth and Coupling Efficiency. *International Journal of Infrared and Millimeter Waves* **24**(1), 261–284 (2003) <https://doi.org/10.1023/A:1021903132609>
21. Lin, C.-C., Hwang, Y.-J.: Single-sleeve waveguide-to-microstrip transition probe for full waveguide bandwidth. In: 2012 7th European Microwave Integrated Circuit Conference, pp. 766–769 (2012)
22. Risacher, C., Vassilev, V., Pavolotsky, A., Belitsky, V.: Waveguide-to-microstrip transition with integrated bias-T. *IEEE Microwave and Wireless Components Letters* **13**(7), 262–264 (2003) <https://doi.org/10.1109/LMWC.2003.815182>
23. Li, B., Zhang, J., Deng, Y., Ma, T., Zhou, Z., Sun, L.: W-band Microstrip-to-Waveguide Transition without Back-short Structure. In: 2021 International Conference on Microwave and Millimeter Wave Technology (ICMMT), pp. 1–2 (2021). <https://doi.org/10.1109/ICMMT52847.2021.9618261>
24. Llorente-Romano, S., Dorta-Naranjo, B.P., Perez-Martinez, F., Salazar-Palma, M.: Design, Implementation and Measurements of Ka-band Waveguide-to-microstrip Transitions. In: 2002 32nd European Microwave Conference, pp. 1–4 (2002). <https://doi.org/10.1109/EUMA.2002.339378>

25. Oh, H.-S., Yeom, K.-W.: A full ku-band reduced-height waveguide-to-microstrip transition with a short transition length. *IEEE Transactions on Microwave Theory and Techniques* **58**(9), 2456–2462 (2010) <https://doi.org/10.1109/TMTT.2010.2058251>
26. Kumar, G.A., Poddar, D.R.: Broadband Rectangular Waveguide to Suspended Stripline Transition Using Dendritic Structure. *IEEE Microwave and Wireless Components Letters* **26**(11), 900–902 (2016) <https://doi.org/10.1109/LMWC.2016.2615009>
27. Carpenter, J., Iono, D., Kemper, F., Wootten, A.: The ALMA Development Program: Roadmap to 2030 (Monthly Newsletter of International URSI Commission J, Radio Astronomy January 2020, eprint=2001.11076, primaryClass=astro-ph.IM, archivePrefix=arXiv). <https://arxiv.org/ftp/arxiv/papers/2001/2001.11076.pdf>
28. Fuller, G.A., Avison, A., Beltran, M., Casasola, V., Caselli, P., Cicone, C., Costagliola, F., Breuck, C.D., Hunt, L., Jimenez-Serra, I., Laing, R., Longmore, S., Massardi, M., Mroczkowski, T., Paladino, R., Ramstedt, S., Richards, A., Testi, L., Vergani, D., Viti, S., Wagg, J.: The Science Case for ALMA Band 2 and Band 2+3 (2020)
29. González, A., Kojima, T., Kaneko, K., Asayama, S.: 275–500 GHz waveguide diplexer to combine local oscillators for different frequency bands. *IEEE Transactions on Terahertz Science and Technology* **7**, 669–676 (2017)
30. Masui, S., Yamasaki, Y., Ogawa, H., Kondo, H., Yokoyama, K., Matsumoto, T., Minami, T., Okawa, M., Konishi, R., Kawashita, S., Konishi, A., Nakao, Y., Nishimoto, S., Yoneyama, S., Ueda, S., Hasegawa, Y., Fujita, S., Nishimura, A., Kojima, T., Uemizu, K., Kaneko, K., Sakai, R., González, A., Uzawa, Y., Onishi, T.: Development of a new wideband heterodyne receiver system for the Osaka 1.85 m mm-submm telescope: Receiver development and the first light of simultaneous observations in 230 GHz and 345 GHz bands with an SIS-mixer with 4–21 GHz IF output **73**(4), 1100–1115 (2021) <https://doi.org/10.1093/pasj/psab046> arXiv:2105.07786 [astro-ph.IM]
31. Yagoubov, P., Mroczkowski, T., Belitsky, V., Cuadrado-Calle, D., Cuttaia, F., Fuller, G.A., Gallego, J.-D., Gonzalez, A., Kaneko, K., Mena, P., Molina, R., Nesti, R., Tapia, V., Villa, F., Beltrán, M., Cavaliere, F., Ceru, J., Chesmore, G.E., Coughlin, K., Breuck, C.D., Fredrixon, M., George, D., Gibson, H., Golec, J., Josaitis, A., Kemper, F., Kotiranta, M., Lapkin, I., López-Fernández, I., Marconi, G., Mariotti, S., McGenn, W., McMahon, J., Murk, A., Pezzotta, F., Phillips, N., Reyes, N., Ricciardi, S., Sandri, M., Strandberg, M., Terenzi, L., Testi, L., Thomas, B., Uzawa, Y., Viganò, D., Wadefalk, N.: Wideband 67–116 GHz receiver development for ALMA band 2. *Astronomy & Astrophysics* **634**, 46 (2020) <https://doi.org/10.1051/0004-6361/201936777>
32. Williams, D., Jargon, J., Arz, U., Hale, P.: Rectangular-Waveguide Impedance. Automatic RF Techniques Group Microwave Measurements Conference, Phoenix, AZ, 2015. <https://doi.org/10.1109/ARFTG.2015.7162902>
33. Escudero, J., Torres, A., Gonzalo, R., Ederra, I.: A simplified design inline microstrip-to-waveguide transition. *Electronics* **7**, 215 (2018) <https://doi.org/10.3390/electronics7100215>
34. Villegas, F.J., Stones, D.I., Hung, H.A.: A novel waveguide-to-microstrip transition for millimeter-wave module applications. *IEEE Transactions on Microwave Theory and Techniques* **47**(1), 48–55 (1999) <https://doi.org/10.1109/22.740075>
35. Li, J., Ying, Q., Xu, J.: A full K-band microstrip-to-waveguide transition using tapered CPS probe and V-antenna. In: 2012 The 7th German Microwave Conference, pp. 1–4 (2012)
36. Guo, J., Xu, J., Cui, Y., Xu, Z., Qian, C.: Q-band waveguide-to-suspended-stripline transition with DC/IF. In: 2014 Asia-Pacific Microwave Conference, pp. 283–285 (2014)
37. Chakrabarti, S., Chatterjee, S., Banerjee, P.: An unconventional design of microstrip to waveguide ridged transition at K-band. In: 2017 IEEE Applied Electromagnetics Conference (AEMC), pp. 1–2 (2017). <https://doi.org/10.1109/AEMC.2017.8325752>
38. Han, K.Y., Pao, C.-k.: A V-band waveguide to microstrip inline transition. In: 2012 IEEE/MTT-S International Microwave Symposium Digest, pp. 1–3 (2012). <https://doi.org/10.1109/MWSYM.2012.6259752>
39. Mohamed, I., Sebak, A.: Broadband transition of substrate-integrated waveguide-to-air-filled rectangular waveguide. *IEEE Microwave and Wireless Components Letters* **28**(11), 966–968 (2018) <https://doi.org/10.1109/LMWC.2018.2871330>
40. G-logowski, R., Zurcher, J.-F., Peixeiro, C., Mosig, J.R.: Ka-band rectangular waveguide to suspended stripline transition. *IEEE Microwave and Wireless Components Letters* **23**(11), 575–577 (2013) <https://doi.org/10.1109/LMWC.2013.2281408>

41. Mozharovskiy, A., Churkin, S., Arternenko, A., Maslennikov, R.: Wideband Probe-Type Waveguide-To-Microstrip Transition for 28 GHz Applications. In: 2018 48th European Microwave Conference (EuMC), pp. 113–116 (2018). <https://doi.org/10.23919/EuMC.2018.8541511>
42. Wu, Y., Zeng, Q.S.: Design of Rectangular Waveguide-to-Microstrip Transition for Millimeter Wave Application. In: 2020 13th UK-Europe-China Workshop on Millimetre-Waves and Terahertz Technologies (UCMMT), pp. 1–3 (2020). <https://doi.org/10.1109/UCMMT49983.2020.9296094>

**Publisher's Note** Springer Nature remains neutral with regard to jurisdictional claims in published maps and institutional affiliations.

Springer Nature or its licensor (e.g. a society or other partner) holds exclusive rights to this article under a publishing agreement with the author(s) or other rightsholder(s); author self-archiving of the accepted manuscript version of this article is solely governed by the terms of such publishing agreement and applicable law.

## Authors and Affiliations

**Diana Cubillos<sup>1,2</sup> · Camilo Espinoza<sup>3</sup> · David Monasterio<sup>3</sup> · José Pizarro<sup>3</sup> · Leonardo Bronfman<sup>3</sup> · Ricardo Finger<sup>3</sup> · F. Patricio Mena<sup>1,4</sup>**

✉ Diana Cubillos  
diana.cubillos@raig.uchile.cl

Camilo Espinoza  
cespinoz@nrao.edu

David Monasterio  
david.monasterio@raig.uchile.cl

José Pizarro  
jspizarro@u.uchile.cl

Leonardo Bronfman  
leo@das.uchile.cl

Ricardo Finger  
rfinger@u.uchile.cl

F. Patricio Mena  
pmena@nrao.edu

<sup>1</sup> Electrical Engineering Department, Universidad de Chile, Santiago, Chile

<sup>2</sup> Research Department, Universidad ECCI, Bogotá, Colombia

<sup>3</sup> Astronomy Department, University of Chile, Santiago, Chile

<sup>4</sup> Central Development Laboratory, National Radio Astronomy Observatory, Charlottesville, VA, USA